

## Modulation of Size and Shape of Au Nanoparticles Using Amino-X-Shaped Poly(ethylene oxide)–Poly(propylene oxide) Block Copolymers

Sonia Goy-López,<sup>†</sup> Pablo Taboada,<sup>\*,†</sup> Adriana Cambón,<sup>†</sup> Josué Juárez,<sup>†</sup> Carmen Alvarez-Lorenzo,<sup>‡</sup> Angel Concheiro,<sup>‡</sup> and Víctor Mosquera<sup>†</sup>

Grupo de Física de Coloides y Polímeros, Departamento de Física de la Materia Condensada, Facultad de Física, and Departamento de Farmacia y Tecnología Farmacéutica, Facultad de Farmacia, Universidad de Santiago de Compostela, E-15782, Santiago de Compostela, Spain

Received: September 04, 2009; Revised Manuscript Received: November 05, 2009

In the present work, the formation and stabilization of gold nanoparticles in a one-pot water-based synthesis has been achieved in the presence of a four-arm, star-shaped polyoxyethylene–polyoxypropylene (PEO–PPO) block copolymer, Tetronic T904, which acts as both reductant and stabilizer. The influence of several parameters such as copolymer and gold salt concentration, reaction temperature, and solution pH on both the size and shape of the resulting nanocrystals has been established. Low copolymer/gold salt molar ratios favor the formation of either triangular or hexagonal planar nanostructures due to a low reduction rate which turns the reaction into kinetic control. As the molar ratio increases, reduction becomes faster with the subsequent increase in the number of crystal seeds and, thus, the decrease in particle size. In addition, there is an increase in the reduction rate which causes the reduction reaction to be governed by thermodynamics, and consequently, spherical geometries are favored. A particle spherical shape can also be promoted as a consequence of the accumulation of block copolymer molecules on different crystallographic planes, homogenizing the metal surface structure and disabling the growth in different crystallographic directions. The same behavior was observed when the reaction temperature was raised. The size and shape of gold nanoparticles could also be controlled by varying the pH of the medium. As the pH becomes more acidic, protons prevent the oxyethylene part of the copolymer from the reduction of metal ions, and consequently, the number of nuclei decreases. This explains the overall increase in the particle size and the change in shape when the synthesis is carried out in acid medium. Finally, comparison with nanoparticles obtained in the presence of a structurally related linear block copolymer Pluronic P105, with a similar number of EO and PO units as T904, denoted an important incidence of the arrangement of PEO and PPO blocks on the reduction reaction rate and the size and shape of the resulting nanoparticles.

### 1. Introduction

Among all nanostructured materials, Au nanoparticles (Au NPs) with sizes ranging from 1.5 to 100 nm are probably the most extensively studied owing to their intriguing properties and fascinating applications.<sup>1</sup> Their excellent chemical stability, biocompatibility, surface plasmon resonance effect, and unique catalytic activity have enabled a broad range of applications in areas, such as biomedicine and drug delivery,<sup>2</sup> electronics,<sup>3</sup> information storage,<sup>4</sup> and photovoltaic devices.<sup>5</sup> Since the properties of Au NPs extensively depend on their dimensions, composition, crystallinity, shape, and construction geometry (e.g., core–shell, solid, or hollow), an exquisite shape and size control of Au nanocrystals is, therefore, highly desirable for tailoring their properties and for improving the performance in many applications. Particularly, size and shape have been shown critical for the *in vivo* biodistribution, targeting, cellular internalization, vascular dynamics, and clearance of nanoparticles.<sup>6</sup>

Although no generalized metal nanoparticle synthetic routes and mechanisms have been reported so far, several methods have been shown useful for controlling the size and shape of

Au nanocrystals through the selection of reductants, stabilizers, and reaction conditions. Some research groups have led pioneering efforts toward the rational control of the structure of Au NPs: Murphy et al. have reported a seeded-mediated growth process to derive multiple shapes of gold nanoparticles such as rods, hexagons, cubes, and branched structures;<sup>7,8</sup> Yang et al.,<sup>9</sup> Scherer et al.,<sup>10</sup> Song et al.,<sup>11</sup> Liz-Marzán et al.,<sup>12</sup> and Hamley et al.<sup>13</sup> made use of modified polyol processes to synthesize different polyhedral and branched Au NPs. However, most of these preparations use organic solvents and/or toxic reagents. Compared to these methods, a green water-based approach should provide a more environmentally sound route to the production of Au nanocrystals. High-purity water is more readily accessible than an organic solvent, and the risk of unexpected results that might be caused by trace amounts of impurities can be minimized. The combination of synthesis in aqueous medium with the use of safe and easy-to-handle reductants and stabilizers such as ascorbic acid,<sup>14</sup> citric acid,<sup>14–16</sup> some alcohols,<sup>17</sup> polymers,<sup>18–20</sup> or proteins<sup>21,22</sup> provides on one hand an easy adjustment of the reduction kinetics and, on the other, the direct applicability of the resulting gold nanostructures in biological and biomedical applications.<sup>23,24</sup> A water-based system has the additional advantages of simplicity, convenience, and potential for large-scale production.<sup>14</sup> For all these reasons, in the past years several research groups have paid special attention to

\* To whom correspondence should be addressed. E-mail: pablo.taboada@usc.es.

<sup>†</sup> Facultad de Física.

<sup>‡</sup> Facultad de Farmacia.

green-water-based synthetic routes of Au NPs using nontoxic polymers as both reductants of the gold salt and capping agents of the gold nanocrystals. The polymer structure, molecular weight, and concentration allowed fine and easy tuning of the size and shape of the resulting nanoparticles. For example, Xia et al.<sup>25,26</sup> and López-Quintela et al.<sup>27,28</sup> have reported on the synthesis of gold spherical and branched nanoparticles, nanoplates, nanotadpoles, and nanokites by reducing HAuCl<sub>4</sub> with poly(vinylpyrrolidone) (PVP), which also acts as a capping agent. Alexandridis et al.<sup>29,30</sup> and Liu et al.<sup>31</sup> have prepared spherical and polyhedral gold nanoparticles by reduction and stabilization of a Au salt with various Pluronic copolymers [poly(ethylene oxide)-poly(propylene oxide)-poly(ethylene oxide), PEO<sub>x</sub>-PPO<sub>y</sub>-PEO<sub>x</sub>, *x* and *y* being the block lengths], and Goy-López et al.<sup>32</sup> described the obtaining of size-tunable Au nanoplates by reduction and stabilization of HAuCl<sub>4</sub> using poly(ethylene oxide)-poly(styrene oxide)-poly(ethylene oxide), PEO<sub>x</sub>-PSO<sub>y</sub>-PEO<sub>x</sub>, block copolymers.

Here, we report on the formation of Au NPs and the control of their size and shape by using a commercially available poloxamine block copolymer (Tetronic from BASF). Differently from their linear counterparts Pluronic copolymers, Tetronics have an X-shaped structure made of an ethylenediamine central group bonded to four chains of PPO-PEO blocks. The unique structure of poloxamines makes them multistimuli responsive, widening their scope of biomedical and pharmaceutical applications.<sup>33</sup> In this context, the two tertiary amine central groups play an essential role in conferring thermodynamical stability and pH sensitivity.<sup>34-36</sup> As a result of the responsiveness of the block copolymer, controlled variations in solution conditions such as pH, temperature, polymer, and Au concentration may remarkably modify the role of Tetronics as both reductant and capping agents in the gold reduction reaction. Thus, the aim of this work was to analyze the effect of these variables on the reduction kinetics and the size and shape of the resulting metal nanoparticles to elucidate the potential of Tetronics in the Au NP field. In addition, the role of the X-shaped structure of Tetronic T904 in the size and shape evolution of gold nanoparticles was also elucidated when compared to those nanocrystals obtained by using a Pluronic block copolymer counterpart with relative similar total block lengths, Pluronic P105.

## 2. Experimental Section

**2.1. Materials.** Tetronic T904 ((OE<sub>15</sub>OP<sub>17</sub>)<sub>2</sub>NCH<sub>2</sub>CH<sub>2</sub>N-(OP<sub>15</sub>OE<sub>17</sub>)<sub>2</sub>) was a gift from BASF Corporation (USA) and used as received (see Figure S1 in Supporting Information for molecular structure scheme). HAuCl<sub>4</sub>·3H<sub>2</sub>O (99.9% purity) was purchased from Sigma Chemical Co. (USA) and used without further purification. Water used in all reactions was doubly distilled and degassed before use.

**Synthesis of Nanoparticles.** Gold nanoparticles were prepared by mixing HAuCl<sub>4</sub> aqueous solutions (0.2 mL) of desired concentrations with block copolymer aqueous solutions (2 mL) of suitable concentrations at certain temperatures. The reported copolymer concentrations hereafter are those at final systems, i.e., after mixing with the HAuCl<sub>4</sub> solution. Solutions were vigorously stirred for 2 min and then kept at suitable temperature in a thermostatted water bath.

**2.2. Characterization of Gold Nanoparticles.** The evolution of the gold reduction and the optical properties of the prepared Au NPs in the aqueous medium were characterized by UV-vis spectrophotometry (Beckman DU series 640). Morphologies of the NPs were observed with a transmission electron microscope (Phillips CM-12) operated at 120 kV. To prepare most of the

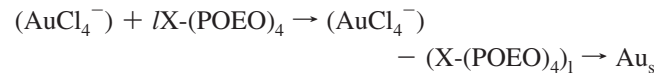
TEM samples, the reaction mixture was centrifuged three times (6000 rpm for 30 min); the supernatant containing unreduced ions and copolymer molecules in excess was removed; and the solid residue was redispersed again in water. Then, a little drop of the resulting dispersion was put onto a carbon-covered copper grid and slowly dried on air. The size distribution of the gold nanoparticles was obtained by measuring the diameter of at least 200 particles viewed in the micrographs. Electron diffraction patterns (SAED) were recorded by high-resolution electron microscopy (JEM-2010, JEOL Ltd.) in conventional transmission mode, operating at 200 kV. X-ray diffraction analysis of the solid Au NPs was carried out using a Siemens D5005 X-ray diffractometer with a rotating anode X-ray generator. Twin Göbel mirrors were used to produce a well-collimated beam of Cu K $\alpha$  radiation ( $\lambda = 1.5418 \text{ \AA}$ ). Samples were put into capillaries with a diameter of 0.5 mm. X-ray diffraction patterns were recorded with an imaging plate detector AXS F.Nr. J2-394.

## 3. Results and Discussion

### 3.1. Effect of Gold Salt/Block Copolymer Molar Ratio.

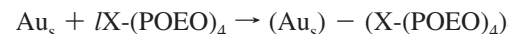
The formation of Au NPs by mediated-block copolymer synthesis comprised three main steps as previously elucidated:<sup>29</sup>

(a) Reduction of Au(III) ions by the block copolymer, via oxidation of the EO and PO segments by the metal center<sup>35</sup> in bulk solution, resulting in the formation of gold clusters (Au<sub>s</sub>) as follows



where  $(\text{AuCl}_4^-) - (\text{X-(POEO)}_4)_l$  represents  $\text{AuCl}_4^-$  ions bound to cavities formed from hydrated EO and PO coils and X indicates the X-shape of the copolymer.

(b) Adsorption of block copolymers on the surface of metal clusters and subsequent reduction of metal ions on the surface of these gold clusters, which involves particle growth



where  $(\text{Au}_s) - (\text{X-(POEO)}_4)_l$  represents a gold cluster with adsorbed copolymer which can form pseudocrown ether structures that bond further with  $\text{AuCl}_4^-$  ions,  $(\text{Au}_s) - (\text{X-(POEO)}_4)_l - (\text{AuCl}_4^-)$ , and facilitate their reduction.

(c) Colloidal stabilization of the resulting metal nanoparticles by the block copolymer molecules.

Size and shape of metal nanoparticles are typically determined by competition between nucleation (metal ion reduction in bulk) and growth (metal ion reduction on nuclei) processes. Namely, if metal ion reduction in bulk solution is more dominant than on nuclei and/or on small particles, new particle formation (number increase) is more significant than particle growth (size increase). Alternately, if metal ion reduction occurs on nuclei and/or on small particles more dominantly than in bulk solution, then particle growth is more significant. Particle formation and growth are controlled by the amphiphilic (dual-nature) character of the block copolymer: ethylene oxide enhances  $\text{AuCl}_4^-$  reduction in solution, whereas propylene oxide enhances copolymer adsorption on nanoparticle surfaces. This results in a competition between  $\text{AuCl}_4^-$  reduction in the bulk solution (which leads to an increase in the number of particles) and on the particle surface (which causes an increase in particle size).<sup>30</sup> Then, we examined the effect of T904/AuCl<sub>4</sub><sup>-</sup> molar ratio on the size and shape of resulting gold nanoparticles. The gold salt concentration was fixed at 0.5 mM, and the copolymer

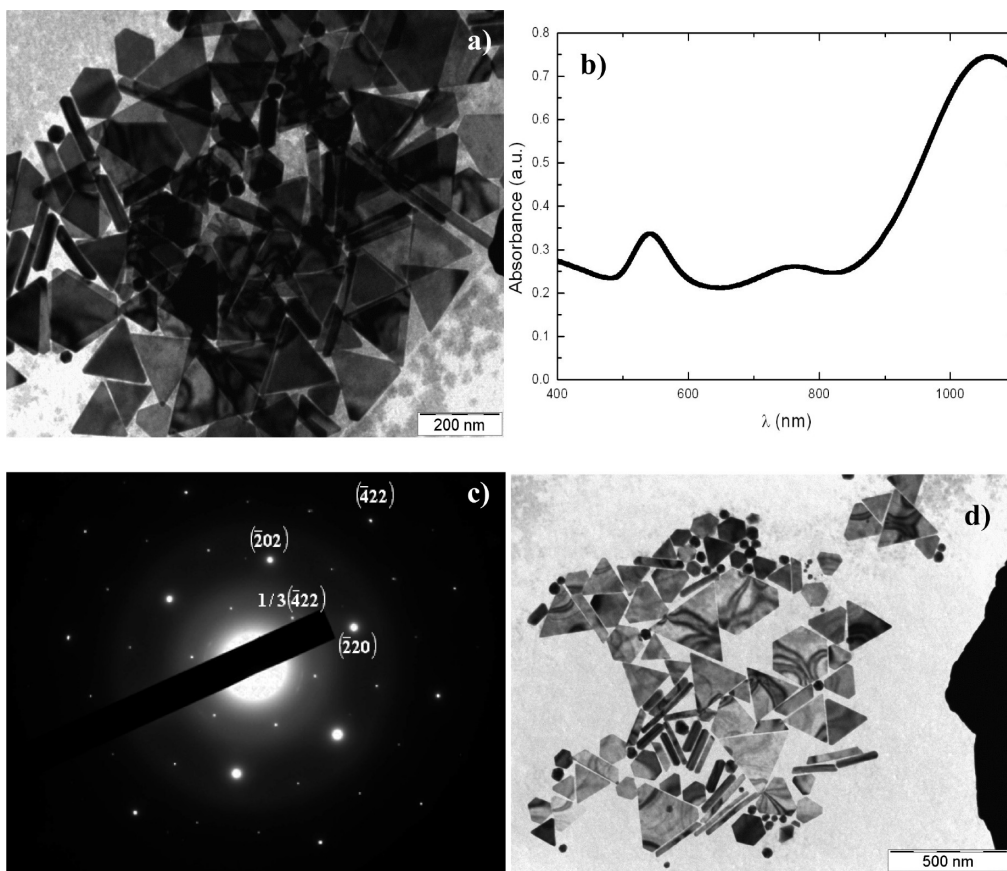


**Figure 1.** (a) TEM image of gold nanoplates formed by reduction of  $\text{HAuCl}_4$  in the presence of T904 at a copolymer/metal salt molar ratio (MR) of 1.5 (0.5 mM  $\text{HAuCl}_4$ ) at 25 °C. (b) Absorption spectrum of the nanoplates. (c) SAED pattern taken from an individual nanoplate and its assigned reflection indexes. (d) TEM image of gold nanoplates displaying bending contours.

concentration varied between 0.25 and 35 mM. Several regions in terms of the size and shape of the resulting Au NPs were found: (a) At low molar ratio (MR), between 0.5 and 1.5, the color of the solutions evolved from light yellow to pink and then to blue tint, thereby indicating the predominant formation of Au nanoplates, as will be shown below; (b) at MR between 1.5 and 3.0, a progressive decrease in the number of nanoplates took place, and the presence of spheroidal particles of sizes of ca. 40 nm increased; and (c) at MR between 3.0 and 70, formation of almost perfect spherical nanoparticles occurred, whose sizes progressively diminished from 40 to 5 nm as the copolymer/gold salt MR increased.

**3.1.1.  $\text{MR} = 0.5\text{--}1.5$ .** Figure 1a shows TEM images of the gold triangular and hexagonal nanoplates obtained at  $\text{MR} = 1.5$ . The reaction yield was ca. 70%, and the mean lateral sizes were  $\sim 174 \pm 40$  nm. Some nanobelts with sizes of  $\sim 200$  nm in length can be also observed in the image. Nanoplates were also obtained at  $\text{MR} = 0.5$  and 1.0 with similar yields, although a larger size variability was found. The nanoplates are characterized by an absorption spectrum (Figure 1b) with a band centered at  $\sim 1000$  nm, which corresponds to the in-plane resonance of the triangular planar objects. Since this peak is very sensitive to snipping, and provided that an important part of the plates does not show acute edges, the absorption maximum is blue-shifted if compared to that of a perfect sharp plate of equivalent size. The broadband at  $\sim 750$  nm should correspond to the in-plane quadrupole mode of the nanoplates based on the prediction of the discrete dipole approximation,<sup>37,38</sup> whereas the band at  $\sim 540$  nm relates to the out-of-plane quadrupole resonance of the nanoplates combined with the plasmon band of spherical

nanoparticles also formed in solution, which display mean sizes of ca. 40 nm.

As shown previously,<sup>25,35,37,38</sup> SAED patterns of nanoplates reveal a regular, hexagonal, diffraction spot array that corresponds to a (111) zone-axis single crystal with an atomically flat surface (see Figure 1c). Bragg diffractions spots of {220}, {422}, and inner 1/3 {422} (lattice spacing of 1.4, 0.8 Å, and 2.4 Å, respectively) are displayed, and the latter is forbidden in a typical fcc single-crystal structure and often associated with thin structures enclosed by atomically flat top and bottom facets bound by {111} planes.<sup>37,38</sup> The X-ray diffraction pattern (XRD) recorded from the same sample shows sharp peaks corresponding to {111}, {200}, {220}, and {311} diffraction peaks of metallic Au, and thus, it indicates that the precipitate is composed of pure crystalline Au. The intensity ratios of the (200) and (220) peaks to the (111) peak were much lower than the bulk value (0.15 and 0.11 versus 0.52 and 0.32), indicating that nanoplates were dominated by {111} facets (see Figure S2 in Supporting Information). The flat nature of nanoplates can be demonstrated, for example, by the low contrast observed for the polygonal particles. The plates are also decorated with different bending contours, diffraction effects resulting from slight bending of thin nanoplates as a consequence of some structural instability of these nanobuilding blocks (see Figure 1d).<sup>39</sup>

Nanoplate formation seems to be favored at low MRs due to both the mild reducing power and the low concentration of the block copolymer, which involve a decrease in the reaction rate, turning it into kinetic control. The rate of creation of new metal nuclei in solution decreases, and possible selective copolymer adsorption on {111} planes of the nanocrystals due to their

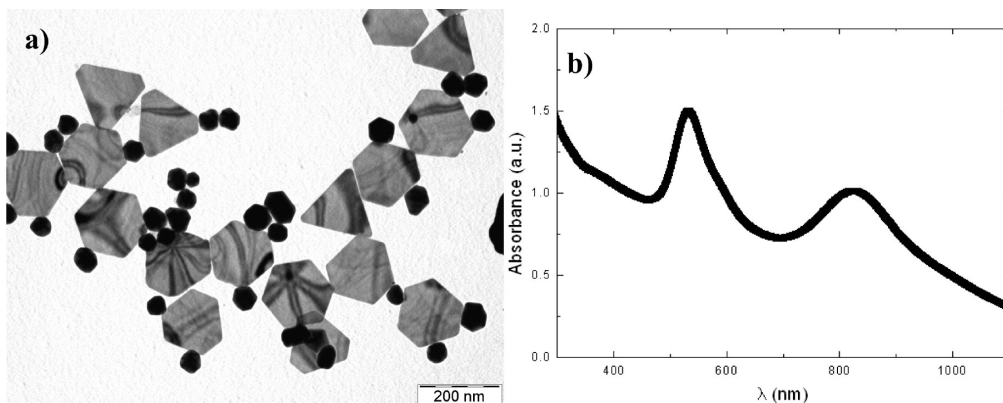


**Figure 2.** (a) TEM image of gold nanoparticles formed by reduction of  $\text{HAuCl}_4$  in the presence of T904 at a copolymer/metal salt molar ratio (MR) of 2.5 (0.5 mM  $\text{HAuCl}_4$ ) at 25 °C. (b) Absorption spectrum of the sample.

lowest energy occurs, which inhibits the growth on such crystallographic planes and promotes anisotropic growth along the {110} orientation by Au atomic attachment. Then, this leads to the formation of (111) bounded structures as thin nanoplates.<sup>32,38</sup> The presence of some nanobelts may also indicate the existence of a secondary mechanism of particle formation: some small previously formed triangular nanosheets with similar sizes might either be connected into a long and thin nanobelt along the <110> direction (which should be thermodynamically more stable) or become attached along the {110} lateral planes, which are of relatively high surface energy, leading to the formation of larger triangular or hexagonal nanoplates.<sup>40,41</sup>

On the other hand, we cannot disregard the role of the etchant  $\text{O}_2/\text{Cl}^-$  pair to eliminate twinned particles and favor nanoplate formation (via a decrease in the reaction rate).<sup>25</sup> In fact, if the reaction is made under an inert  $\text{N}_2$  atmosphere, the hexagonal and triangular nanoplate yield decreases, and more rounded nanoplates and spherical nanoparticles are obtained (see Figure S3, Supporting Information).

**3.1.2. MR = 1.5–3.0.** As MR increases in this region, a decrease of Au nanoplates and a progressive increase in the number of spheroidal particles takes place. Figure 2a shows TEM images of a gold solution at MR = 2.5, in which faceted-rounded particles of mean diameter of  $40 \pm 8$  nm are formed. Nanoplates of different sizes are also observed at lower yields ( $\sim 45\%$ ). This is also confirmed by the UV–vis spectrum, which displays a maximum centered at 530 nm (see Figure 2b). A very broad and low band centered at 850 nm evidenced the relative low concentration of Au nanoplates.

The presence of a slightly larger copolymer concentration implies that  $\text{AuCl}_4^-$  reduction starts to occur preferably in bulk solution, so complete kinetic control is not achieved. This enhances the accumulation of the block copolymer molecules on different crystallographic planes homogenizing the metal surface structure and preventing the differential growth in different crystallographic directions. Thus, spherical nanoparticles are progressively formed.

**3.1.3. MR > 3.0.** As the copolymer/metal salt MR further increases, the growth in T904 concentration leads to a progressively more efficient reduction reaction as denoted by the increase in the net absorbance of Au NPs (see Figure S4, Supporting Information). The increase in the number of copolymer molecules in solution seems to favor the pseudocrown cavity formation around  $\text{AuCl}_4^-$  ions, in which reduction of bound  $\text{AuCl}_4^-$  proceeds via oxidation of PEO chains by the metal ion, over geometrical constraints due to micelle formation

and excluded volume effects from one micelle to other provided that we are at concentrations above the critical micelle concentration (CMC) of the block copolymer.<sup>34,35</sup> It is worth mentioning that the formation of pseudocrown ether structures is caused by ion–dipole interactions between metal ions and PEO chains. This situation favors the formation of new nuclei in solution over reduction on the surface of previously formed metal clusters, which involves an increase in the number of particles and a decrease in their size.<sup>32,40</sup> In addition, the presence of larger amounts of copolymer molecules also helps, providing a better stabilization of the resulting particles and, thus, limiting their size as observed for other colloidal systems.<sup>42</sup> TEM images of spherical particles obtained at different MRs (Figure 3) corroborate these findings. As MR becomes larger, the Au NP size decreases, with diameters as small as 5 nm and excellent monodispersity (see Figure S5, Supporting Information, for size distributions as an example). This is also confirmed by the surface plasmon resonance band centered at ca. 520 nm, which progressively undergoes a slight blue-shift; this band also becomes progressively more intense and narrower as a result of the increase in NP number and a greater monodispersity (Figure 3f). Furthermore, the particles obtained under these conditions possess smaller sizes than those obtained by using diamine-terminated poly(ethylene oxide),<sup>43</sup> aromatic amines,<sup>44</sup> or poly(propyleneimine) dendrimers<sup>45</sup> as both reductant and stabilizing agents.

The crystalline structure of the resulting nanoparticles was confirmed by recording the XRD pattern (see Figure S6, Supporting Information). The intensity ratios of the {200} and {220} peaks to the {111} diffraction peak were slightly lower than the bulk value (0.36 and 0.28 versus 0.52 and 0.32), which indicates a certain predominance of the (111) facets on the formed nanoparticles.

It was also noted that at  $\text{MR} > 16$ , at which the copolymer micellization equilibrium is completely shifted to the formation of aggregates, copolymer micelles loaded with very small gold nanoparticles (2–4 nm) were also formed in solution, coexisting with free slightly larger Au NPs (Figure 4). The presence of the metal salt may additionally reduce the CMC of the block copolymer, thus increasing the number of micelles in solution.<sup>34,35</sup> We hypothesize that the formation of these Au-loaded micelles originates from binding of Au(III) ions to both the diamine polymer core and the cavities formed by the oxyethylene groups, via ion–dipole interactions between the  $\text{AuCl}_4^-$  ions and PEO segments after copolymer dissolution in the gold solution.<sup>46,47</sup> In this way, the metal ions would become entrapped and reduced

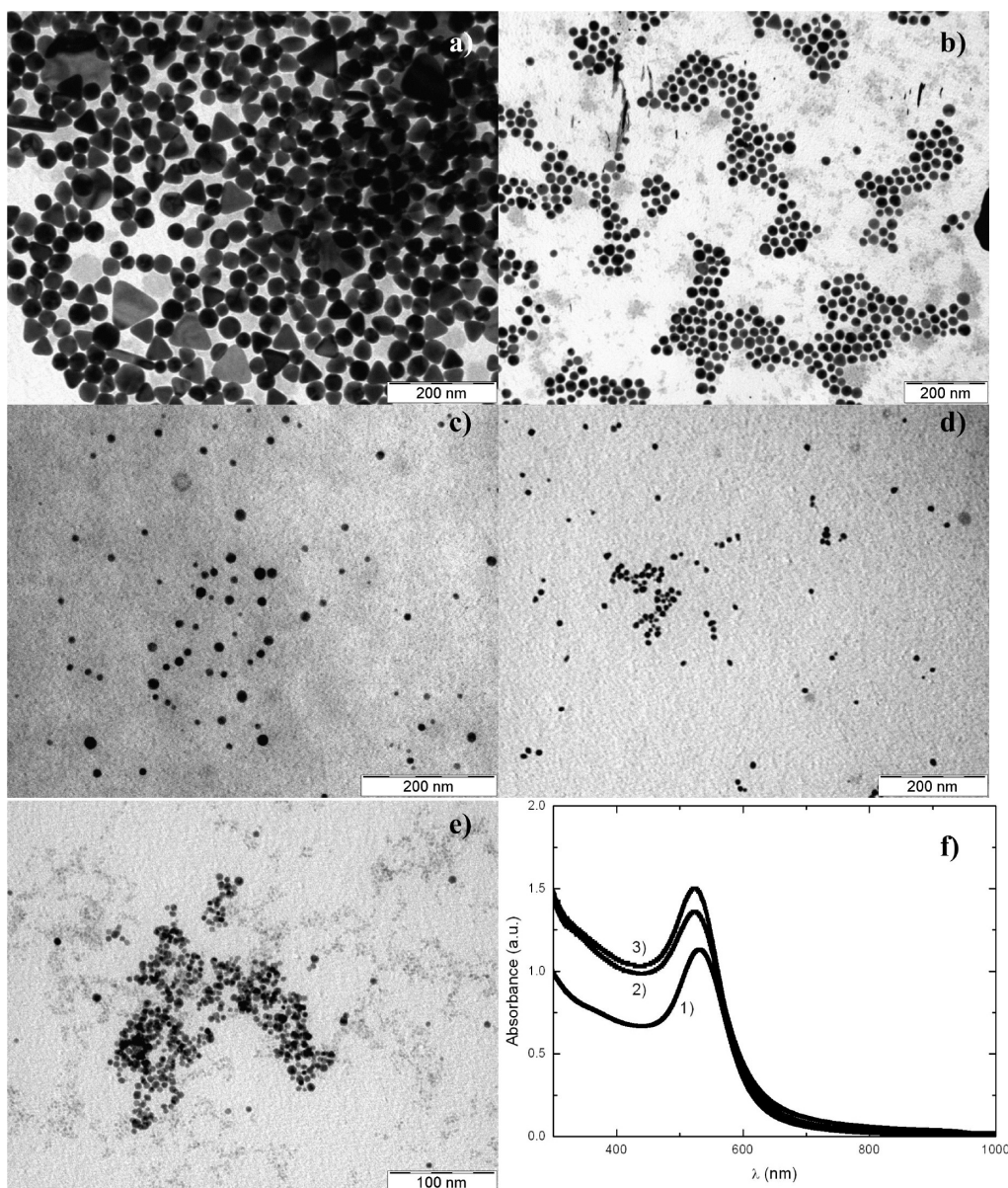


**Figure 3.** TEM images of gold nanoparticles formed by reduction of  $\text{HAuCl}_4$  in the presence of T904 at a copolymer/metal salt MR of (a) 4, (b) 8, (c) 16, (d) 32, and (e) 64 at 25 °C (0.5 mM  $\text{HAuCl}_4$ ). (f) Absorption spectra of samples with MR (1) 4, (2) 16, and (3) 64.

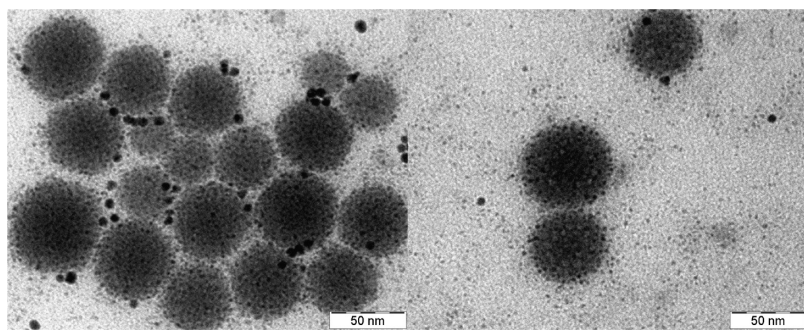


**Figure 4.** Copolymer micelles with gold nanoparticles embedded in their interior at MR > 16 and 25 °C.

in the copolymer micelles. The higher the number of micelles with a loosely packed structure, as in the case of the T904 micelles due to its molecular branching construction, the more favored the penetration of gold ions inside the micelle and their subsequent reduction is. Nevertheless, further studies are being performed to confirm this hypothesis and for isolation and characterization of the hybrid-polymer micelles.

**3.1.4. Growth Mechanism.** To elucidate the growth mechanism of the Au nanoplates and nanoparticles, we monitored the evolution of their shape with TEM by taking samples at various reaction times. Figure 5 shows TEM images of Au nanoplates sampled at 1, 3, 12, and 24 h, respectively, at MR = 2. At  $t = 1$  h, the sample contains tiny gold seeds with sizes less than 5–7 nm, which can be single or twinned nanocrystals.

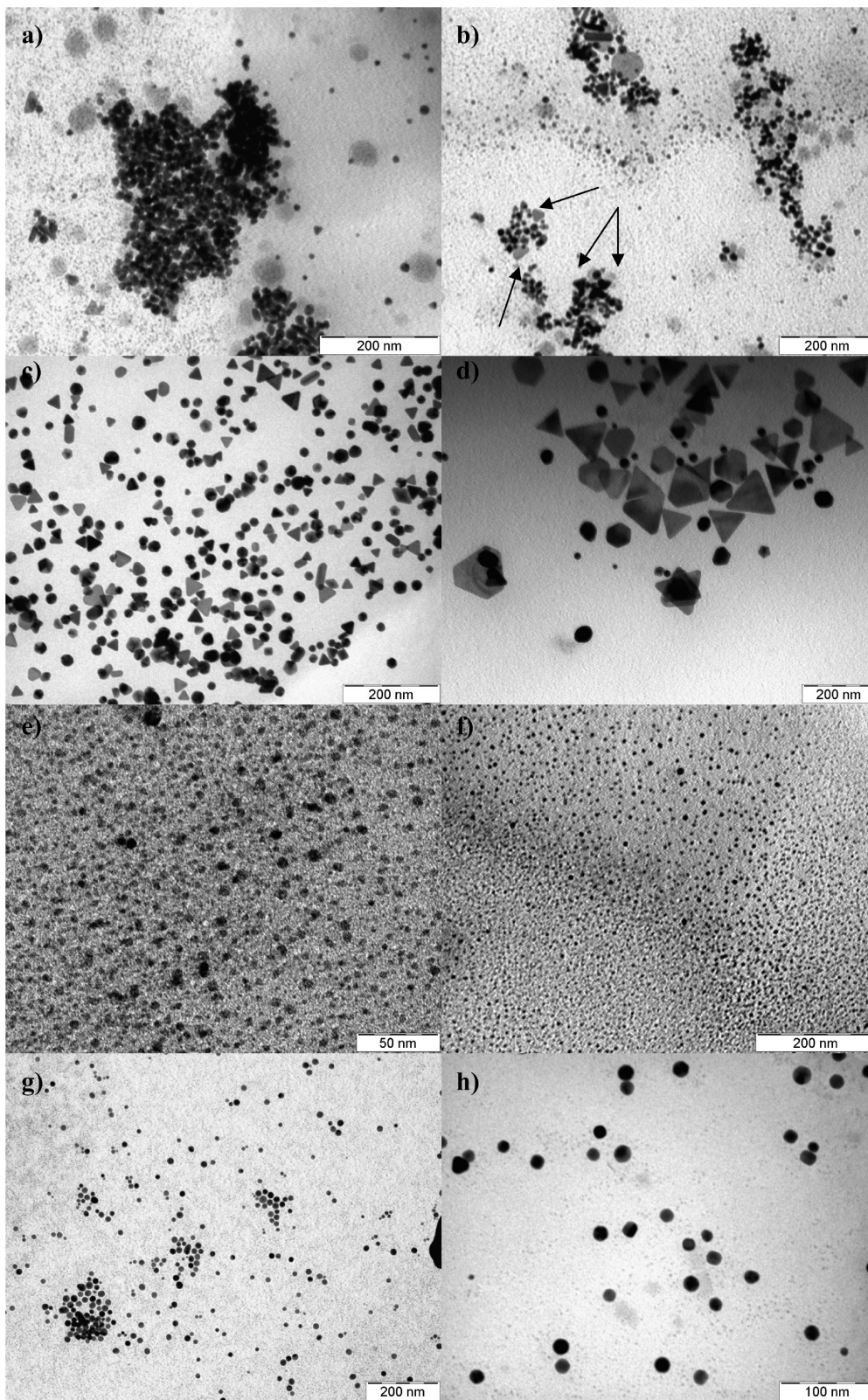


**Figure 5.** TEM pictures showing the time evolution of Au nanoplate (a–d) and Au spherical nanoparticle (e–h) formation at  $MR = 2$  and  $8$ , respectively, at  $25\text{ }^{\circ}\text{C}$  and  $t =$  (a)  $1\text{ h}$ , (b)  $3\text{ h}$ , (c)  $12\text{ h}$ , (d)  $24\text{ h}$ , (e)  $15\text{ min}$ , (f)  $2\text{ h}$ , (g)  $6\text{ h}$ , (h)  $12\text{ h}$ .

At  $t = 3\text{ h}$ , small triangular gold seeds with sizes between  $10$  and  $15\text{ nm}$  start to be observed (Figure 5b, see arrows), although quasispherical ones are predominant, which could be either cubooctahedral or multitwinned particles (MTPs). We cannot distinguish if triangular seeds are planar or not, although the low contrast of some of them might indicate planarity. Some other authors have also reported the formation of triangular seeds

of dimension similar to those of the present work in the early stages of their reactions.<sup>41,48</sup> At  $t = 12\text{ h}$ , nanoplates start to become the main product (Figure 5c), with lateral sizes between  $30$  and  $60\text{ nm}$ . After  $24\text{ h}$ , nanoplates with relatively sharp edges grew to their final sizes of ca.  $150\text{ nm}$ . Most of the small nanocrystals below a certain size have disappeared, while the larger nanoplates have become bigger, thereby suggesting the

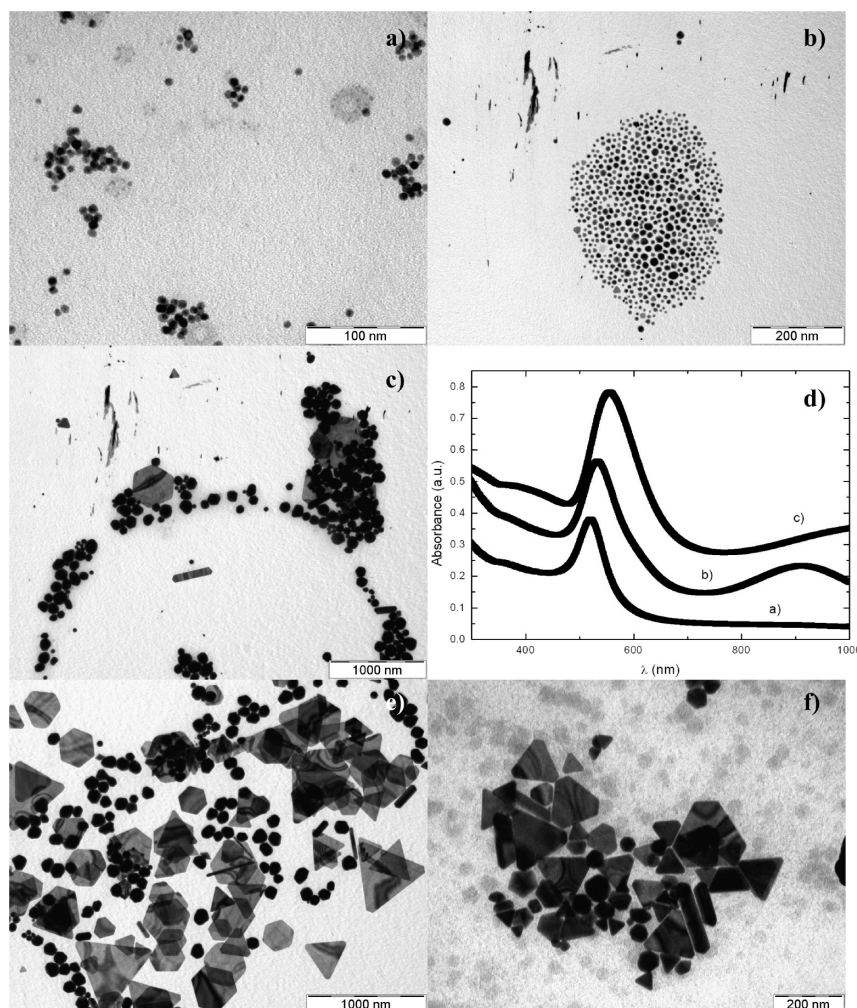


**Figure 6.** TEM images of gold particles formed by reduction of HAuCl<sub>4</sub> in the presence of 1 mM T904 and HAuCl<sub>4</sub> concentrations of (a) 0.06, (b) 0.2, and (c) 0.8 mM at 25 °C. (d) Absorption spectra of the former samples. The absorbance maximum corresponding to nanoplates for the sample at 0.8 mM HAuCl<sub>4</sub> partially lies out of the range of measurement of our instrument. (e) TEM images of gold particles formed by reduction of 2 mM HAuCl<sub>4</sub> in the presence of 1 mM T904. (f) TEM images of gold particles formed by reduction of 0.2 mM HAuCl<sub>4</sub> in the presence of 1 mM T904 and 100 mM NaCl at 25 °C.

involvement of Ostwald ripening in the growth process. In the case of spherical nanoparticles at MR = 8, small seeds can be observed after 30 min after starting the reaction, which evolved to small nanoparticles of sizes around 5–7 nm at  $t = 2$  h (see Figures 5e,f). The nanoparticles progressively increases their sizes until reaching a mean diameter of ca. 20 nm (see Figure 5g,h), probably at the expense of those particles with lower sizes by an Ostwald ripening mechanism as in the case of Au nanoplates.

**3.1.5. Comparison with Copolymer P105.** Although copolymers T904 and Pluronic P105 show relatively similar block lengths, the different arrangement of PPO and PEO blocks may involve dissimilarities in the reduction reaction rate and in the size and shape of the resulting nanoparticles. First, at least a concentration of 0.2 mM P105 is needed to start the gold reduction reaction from 0.1 mM HAuCl<sub>4</sub> solution,<sup>49</sup> whereas for T904 a concentration as low as 0.07 mM is sufficient. The reduction reaction is also more efficient (as denoted, the larger absorbance values at the same copolymer concentrations) and faster in the presence of T904 under similar conditions. This is supported by the presence of planar nanoplates, which involved kinetic control of the reaction and, thus, very low reaction rates, at much larger copolymer/salt MRs for copolymer P105 (MR = 20) than for T904 (MR = 1.5) (see

ref 29 and 45 for P105 and Figure 1 for T904 for further details). This behavior can be related to the X-shape structure of T904 which might facilitate the formation of pseudocrown cavities, formed by the oxyethylene units inside a single copolymer molecule and the presence of reducing amino groups in the copolymer molecule,<sup>44,50</sup> both factors favoring reduction. Additionally, the slightly greater CMC of T904<sup>35</sup> would also enhance the reduction ability of metal ions in bulk solution. It was also found that as the P105 concentration rises from 4 to 30 mM the size of the resulting gold spherical nanoparticles decreases from 64 to 6–8 nm.<sup>31</sup> We observed that as the T904 concentration varies from 0.5 to 35 mM the size of the spherical nanoparticles decreases from ~40 to 5 nm, which denotes a better stabilization capacity of T904 if compared to P105. The X-shape structure of T904 with a diamine core,<sup>43,44</sup> which gives rise to micelles with looser structure, may provide a better coverage of the nanoparticle surface.

**3.2. Effect of Gold Concentration.** Figure 6 shows TEM images of Au NPs obtained in the presence of 1 mM T904 and varying concentrations of HAuCl<sub>4</sub> (between 0.06 and 2 mM). At low gold salt concentrations (0.06–0.25 mM), small monodisperse spherical nanoparticles of mean diameters ranging from 5–6 nm to 10–12 nm were obtained (Figure 6a,b). At larger metal salt concentrations (0.25–0.75 mM), larger and less

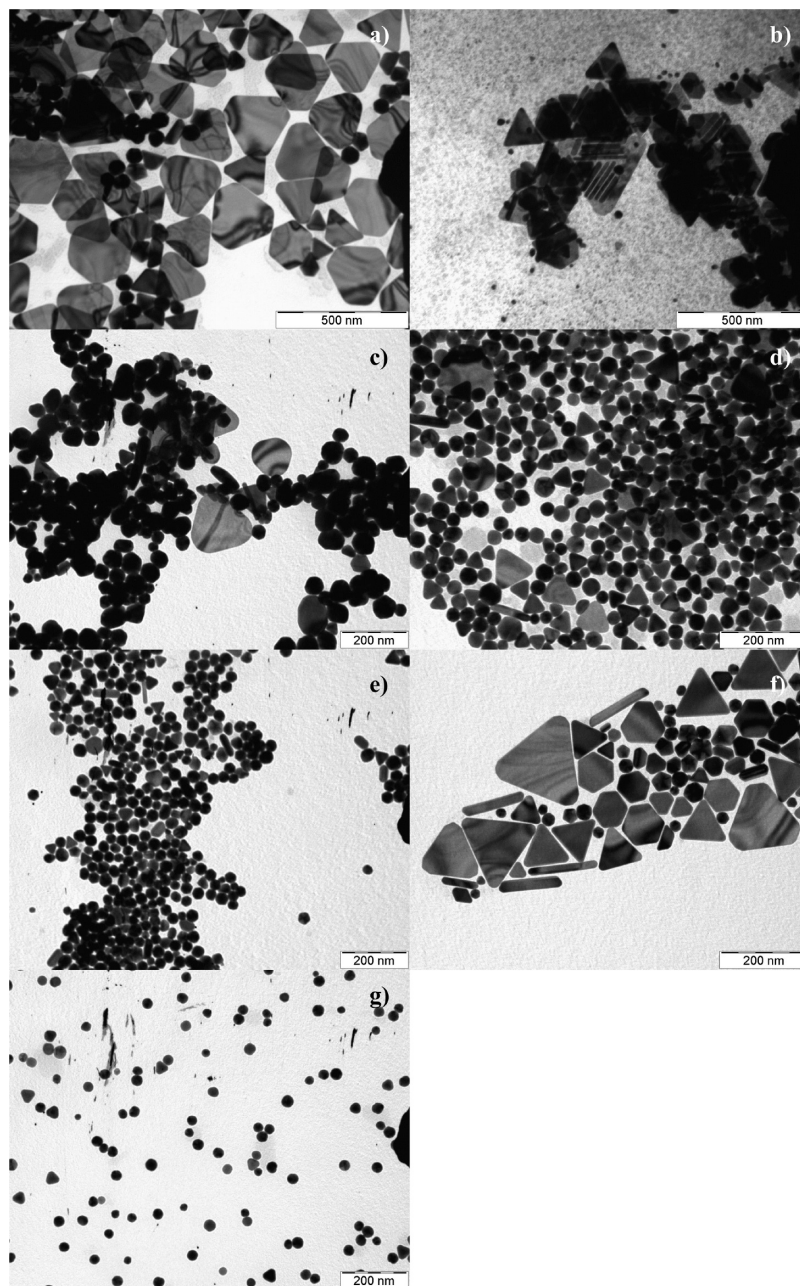


**Figure 7.** TEM images of gold particles formed by reduction of  $\text{HAuCl}_4$  at  $\text{MR} = 4$  (0.5 mM  $\text{HAuCl}_4$ ) and pH (a) 3.0, (b) 4.0, (c) 5.5, (d) 6.5, and (e) 7.5 at 25 °C and at  $\text{MR} = 16$  and pH (f) 3.0 and (g) 7.5 at 25 °C.

spherical particles were formed (Figure 6c). In addition, some triangular plates are already present in solution. This is also confirmed by the appearance of a band with a maximum centered at ca. 900 nm in the absorption spectrum (Figure 6d) which corresponds to the nanoplates and a small red-shift of the band centered at ca. 530 nm as a consequence of the size increase of the resulting spherical nanoparticles. A larger nanoplate population was found when the gold concentration further increased up to 2 mM (Figure 6e). Moreover, the surface plasmon bands of the resulting nanoparticles further red-shifted as metal salt concentration increased (Figure 6d), which points out a certain increase of the particle size as corroborated by TEM. The increasing population of plates as the metal salt concentration rises can be ascribed, on one hand, to a decrease in the reduction rate since the same amount of copolymer molecules has to reduce larger amounts of gold salt and to that the presence of the salt also slightly decreases T904 CMC, which

further makes reduction difficult (data not shown). On the other hand, the adsorption of chloride ions produced during  $\text{HAuCl}_4$  reduction onto specific crystal facets (because  $\text{Cl}^-$  ions prefer to adsorb on gold surfaces<sup>51,52</sup>) can also influence the population of gold plates. This effect has been observed in a recent study when small amounts of halide ions (especially iodide ion) were added to a growth solution with cetyltrimethylammoniumbromide (CTAB).<sup>53</sup> In this regard, when increasing amounts of NaCl are present in the reaction medium, the formation of plates seems to be slightly favored (Figure 5f). Nevertheless, it has to bear in mind that the presence of NaCl also influences the self-assembly behavior of the block copolymer favoring micellization.

At larger gold salt concentrations ( $>2$  mM), certain aggregation of Au NPs occurred due to insufficient block copolymer molecules to correctly stabilize the nanoparticles. In fact, after several days of storage, a metal precipitate could be observed.

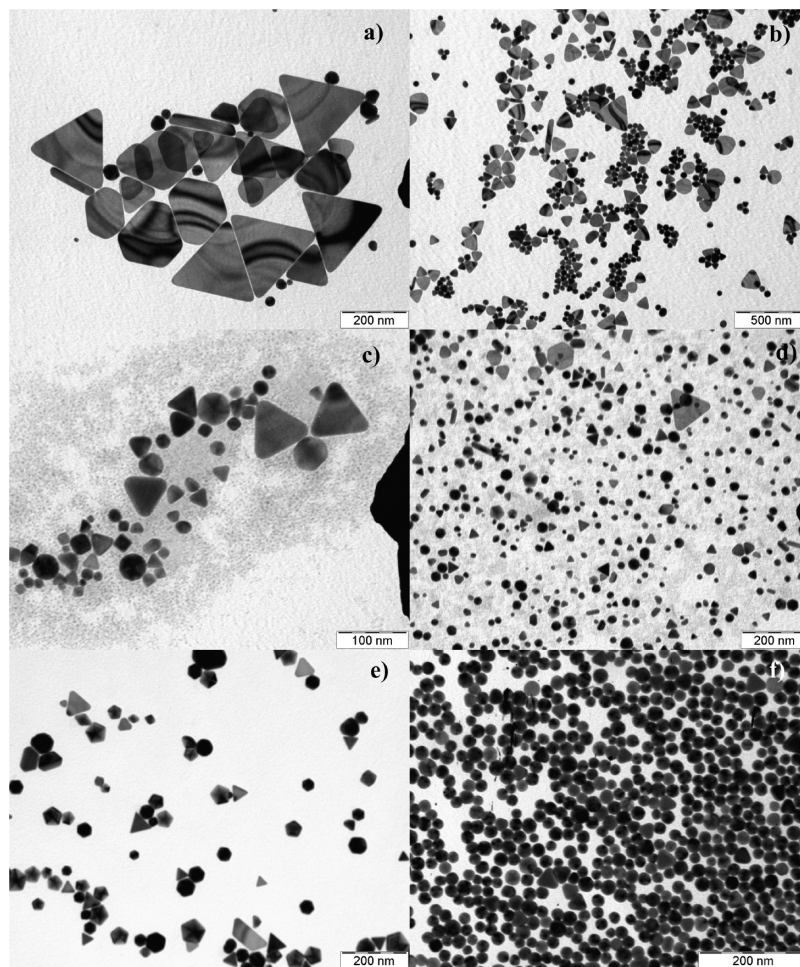


**Figure 8.** TEM images of gold particles formed by reduction of  $\text{HAuCl}_4$  at  $\text{MR} = 1.5$  ( $0.5 \text{ mM } \text{HAuCl}_4$ ) and (a) 35, (b) 45, (c) 60, and (d)  $75^\circ\text{C}$  and at  $75^\circ\text{C}$  for (e)  $\text{MR} = 4$  and (f)  $\text{MR} = 16$ .

**3.3. Effect of pH.** Titration profiles of Tetronic copolymers show two inflection points that correspond to proton dissociation from the two nitrogen atoms on the central ethylene diamine group.<sup>33,34</sup> In the case of T904,  $pK_{\text{a}1}$  and  $pK_{\text{a}2}$  were found to be 4.0 and 8.8, respectively,<sup>35</sup> so the diprotonated form is the predominant one at pH values below 4 and the monoprotonated one predominates between 4.0 and 7.8. The Coulombic repulsions among the positively charged amine groups at the center of the PPO chains constrain self-aggregation, as revealed previously.<sup>34</sup> Thus, as the pH diminishes, the deprotonation–micellization becomes more difficult, leading to an increase in the CMC and to a decrease in micellar size.<sup>34,35</sup> These changes in the behavior of T904 solution as a function of pH should modify the reaction kinetics and, thus, the size and shape of the resulting nanoparticles. Micelles are known to promote polymer entanglements, which decrease the ability of forming the necessary cavities (pseudocrown ether structures) where  $\text{AuCl}_4^-$  ions are bound and reduced via oxidation of the polymer by the metal center.<sup>36</sup> Nucleation becomes a difficult process due to the low supersaturation of Au nuclei formed. Therefore, the size and shape of Au NPs could be controlled by varying the pH of the reaction mixture. Thus, the solution pH was varied by adding suitable amounts of HCl to the reaction mixture. Figure 7 shows selected pictures of the obtained nanoparticles at different pHs and at two copolymer/gold salt MRs, 4 and 16. At  $\text{MR} = 4$ , pH changes between 3.0 and 9.0 involved a variation in both particle size and shape. At pH 3.0, an important population of triangular nanoplates was formed

(yield ca. 60–70%) with lateral sizes  $180 \pm 40 \text{ nm}$ . As the pH increased, the population of these planar objects decreased, and more spherical nanoparticles were formed. The size of the spherical particles also slightly decreased as the pH became higher (Figure 7c–e). These findings were coincident with those obtained for  $\text{MR} = 16$ , except for the yield of planar nanoparticles, which was much lower at the most acidic pH, and for the fact that quasispherical, hexagonal, and triangular forms with sizes below  $\sim 200 \text{ nm}$ , particle edges not well-defined, and an important polydispersity were displayed.

Results similar to those previously mentioned were found when HCl was replaced by  $\text{H}_2\text{SO}_4$  or  $\text{HNO}_3$  (Figure S7, Supporting Information). When similar concentrations of NaCl were used instead of HCl (up to 10 mM), the population of nanoplates was significantly reduced. This behavior clearly indicates that the acid itself exerts a strong influence on the size and shape of the nanoparticles, owing to specific adsorption of  $\text{Cl}^-$  ions on the particle surface. In light of the present results, it seems that the decrease in the micellization degree of the block copolymer due to the protonation of the diamine core is not the main factor for the changes in the size and shape of the nanoparticles. If this were the case, planar plates would not be formed under acidic conditions since these nanostructures emerge when the reduction reaction turns into kinetic control. Thus, additional effects must be considered to explain the observed behavior. At low pH conditions, it is known that  $\text{H}^+$  ions disturb the binding of the metal ions to the oxyethylene groups.<sup>54</sup> Thus,  $\text{H}^+$  ions could prevent the oxyethylene part from

the reduction of metal ions with the consequent decrease in the number of nuclei. This explains the overall increase in the particle size after the addition of acid. Moreover, coordination of gold salt metal ions and protonated amine groups in the copolymer core may also offer an additional protective environment against particle reduction in bulk solution by oxyethylene units which, in fact, involves a depletion of the total free ions concentration available for reduction. This trend is further confirmed when NaOH is added to the solution instead of HCl (Figure S8, Supporting Information). This involves the deprotonation of the diamine core, decreasing its ability to bind free metal ions. The decrease in  $H^+$  ions in solution also favors the binding of metal ions to the oxyethylene groups, increases the reduction rate, and thus promotes the formation of spherical gold nanoparticles in solution. Finally, the pH dependence of the activity of the gold salt, which is lower as the pH becomes more acidic, also influences the resulting size and shape of the nanoparticles.

On the other hand, the presence of more snipped triangular and hexagonal nanoplates at low pH conditions (between pH 3.0–4.0) may also arise from an additional decrease in the reaction rate as a consequence of a lower metal binding by the oxyethylene group. In terms of shape evolution, the nanoplates have a circular cross-section in the initial stage. As the reaction time is prolonged for several hours, they can evolve into hexagonal and then triangular shapes together with an increase in their lateral dimensions if the reduction kinetics is fastened to ensure the appropriate rate of metal addition on the plate surface,<sup>25</sup> which does not seem to be the present case. The extremely slow reaction observed at MR = 16 and pH 3.0 also involves the continuous generation of Au atoms over a long period of time and suppresses Ostwald ripening, which results in the observed important size polydispersity.

**3.4. Effect of Temperature.** To analyze the effect of temperature on the size and shape of Au NPs, we prepared nanoparticle solutions from the reduction of 0.5 mM HAuCl<sub>4</sub> at different copolymer/gold salt MRs in the range of 25–75 °C. For MR = 1.5, a progressive decrease in the number and size of triangular and hexagonal nanoplates occurred as the temperature increased up to 75 °C (see Figure 8a,b). At room temperature, the presence of nanoplates was progressively diminished as MR became larger, and this decrease took place more quickly as the temperature increased.

These changes were also confirmed by absorption spectra. Both nanoplates and spherical nanoparticles coexist in solution as pointed out by the maxima centered at ~1000 and ~530 nm, respectively. There was a progressive decrease in the absorption maximum at ca. 1000 nm and a further increase of the band centered at ca. 530 nm (Figure S9, Supporting Information) as reduction took place at higher temperatures. This behavior is related to an increase in the reduction rate as temperature rises, which means the reduction reaction is under thermodynamic control. In this respect, it has been recently shown by simulation that fcc crystals nuclei formed in the early stages of nucleation tend to take a random hexagonal close-packed (rhcp) structure—a random mixture of both hexagonal close packing (hcp) and cubic close packing—with the inclusion of stacking faults rather than a pure fcc phase. The strain energy caused by stacking faults is so low that the rhcp structure is slightly more stable than fcc at this stage.<sup>14</sup> When the reduction is relatively fast, these nuclei can evolve to polyhedral seeds such as single crystals and 5-fold twinned decahedra in an effort to lower the total surface energy, as observed in the present study.

#### 4. Conclusions

Isotropic and anisotropic gold nanoparticles in good yield have been obtained in aqueous medium by using the amphiphilic four-arm-shaped PPO–PEO block copolymer Tetronic 904. This copolymer acts as both reductant and stabilizer of the reduction reaction of a gold salt, HAuCl<sub>4</sub>. Planar nanostructures were obtained at low copolymer/gold salt molar ratios and/or under acidic conditions, as a consequence of the decrease in the reduction rate which turns the reaction into kinetic control. The rate of creation of new metal nuclei in solution decreases, and the selective copolymer adsorption on {111} planes of the nanocrystals due to their lowest energy occurs. This inhibits the growth on such crystallographic planes and promotes anisotropic growth along {110} orientation by Au atomic attachment leading to the formation of (111) bounded structures as thin nanoplates. Under acidic conditions, protons also disturb the binding of the metal ions to the PEO blocks, and consequently, the reduction rate diminished. An increased population of plates was observed as the metal salt concentration rises. This can be ascribed, on one hand, to the decrease in the reduction rate since the same amount of T904 has to reduce larger amounts of gold salt and to a slight decrease of the CMC and to, on the other hand, the adsorption of chloride ions (Cl<sup>−</sup>) produced during HAuCl<sub>4</sub> reduction onto specific crystal facets. This was corroborated when NaCl was added to the solution. Formation of spherical particles is promoted at larger copolymer/gold salt molar ratios, as a consequence of the accumulation of T904 on different crystallographic planes, which homogenizes the metal surface structure and disables the growth in different crystallographic directions. Spherical particles are also obtained when the reaction temperature increases owing to an increase in the reduction rate, which means the reduction reaction is under thermodynamic control. Comparison between nanoparticles obtained in the presence of T904 with those formed in the presence of P105 denoted an important incidence of the arrangement of PEO and PPO blocks on the reduction reaction rate and the size and shape of the resulting nanoparticles.

**Acknowledgment.** The authors thank Ministerio de Ciencia e Innovación for project MAT-2007-61604 and S.G.-L. for her FPI grant. The authors also thank BASF for the generous gift of the block copolymer.

**Supporting Information Available:** Molecular structure of the copolymer, XRD pattern of Au nanoplates, TEM image of nanoparticles obtained under nitrogen atmosphere, variation of the absorption maxima with copolymer/metal salt molar ratio, size distributions of gold nanoparticles at different copolymer/metal salt molar ratios, XRD pattern of spherical gold nanoparticles, TEM picture of Au nanoplates obtained in the presence of HNO<sub>3</sub> and H<sub>2</sub>SO<sub>4</sub>, TEM citure and UV-vis spectrum of Au nanoparticles obtained in the presence of NaOH, and UV-vis spectra of Au nanoparticles at different temperatures. This material is available free of charge via the Internet at <http://pubs.acs.org>.

#### References and Notes

- (1) Daniel, M. C.; Astruc, D. *Chem. Rev.* **2004**, *104*, 293–346.
- (2) Ghosh, P.; Han, G.; De, M.; Kim, C. K.; Rotello, V. M. *Adv. Drug Delivery Rev.* **2008**, *60*, 1307–1315.
- (3) Pradhan, S.; Sun, J.; Deng, F. J.; Chen, S. *Adv. Mater.* **2006**, *18*, 3279–3283.
- (4) Tseng, R. J.; Huang, J. X.; Ouyang, J.; Kaner, R. B.; Yang, Y. *Nano Lett.* **2005**, *5*, 1077–1080.

- (5) Hasobe, T.; Imahori, H.; Kamat, P. V.; Ahn, T. K.; Kim, S. K.; Kim, D.; Fujimoto, A.; Hirakawa, T.; Fukuzumi, S. *J. Am. Chem. Soc.* **2005**, *127*, 1216–1228.
- (6) Mitragotri, S.; Lahann, J. *Nat. Mater.* **2009**, *8*, 15–23.
- (7) Murphy, C. J.; Sau, T. K.; Gole, A. M.; Orendorff, C. J.; Gao, J.; Gou, L.; Hunyadi, S. E.; Li, T. *J. Phys. Chem. B* **2005**, *109*, 13857–13870.
- (8) Sau, T. K.; Murphy, C. J. *J. Am. Chem. Soc.* **2004**, *126*, 8648–8649.
- (9) Kim, F.; Connor, S.; Song, H.; Kuykendall, T.; Yang, P. *Angew. Chem., Int. Ed.* **2004**, *43*, 3673–3677.
- (10) Jin, R.; Egusa, S.; Scherer, N. F. *J. Am. Chem. Soc.* **2004**, *126*, 9900–9901.
- (11) Seo, D.; Park, C.; Song, H. *J. Am. Chem. Soc.* **2006**, *128*, 14863–14870.
- (12) Kumar, P. S.; Pastoriza-Santos, I.; Rodríguez-González, B.; García de Abajo, F. J.; Liz-Marzán, L. M. *Nanotechnology* **2008**, *19*, 015606/1–015606/6.
- (13) Tang, T.; Hamley, I. W. *Colloid Surf. A* **2009**, *336*, 1–7.
- (14) Lim, B.; Jiang, M.; Tao, J.; Camargo, P. H. C.; Zhu, Y.; Xia, Y. *Adv. Funct. Mater.* **2009**, *19*, 189–200.
- (15) Xiong, Y.; McLellan, J. M.; Yin, Y.; Xia, Y. *Angew. Chem., Int. Ed.* **2007**, *46*, 790–794.
- (16) Lim, B.; Xiong, Y.; Xia, Y. *Angew. Chem., Int. Ed.* **2007**, *46*, 9279–9282.
- (17) Liz-Marzán, L. M.; Lado-Touriño, I. *Langmuir* **1996**, *12*, 3585–3589.
- (18) Ishii, T.; Otsuka, H.; Kataoka, K.; Nagasaki, Y. *Langmuir* **2004**, *20*, 561–564.
- (19) Nisz, K.; Grass, M.; Somorjai, G. A. *Nano Lett.* **2005**, *5*, 2238.
- (20) Piao, Y.; Jang, Y.; Shokouhimehr, M.; Lee, I. S.; Hyeon, T. *Small* **2007**, *3*, 255–260.
- (21) Shanktar, S. S.; Rai, A.; Ankamwar, B.; Singh, A.; Ahmad, A.; Sastry, M. *Nat. Mater.* **2004**, *3*, 482–488.
- (22) Xie, J.; Lee, J. Y.; Wang, D. I. C. *J. Phys. Chem. C* **2007**, *111*, 10226–10232.
- (23) Rossi, N. L.; Mirkin, C. A. *Chem. Rev.* **2005**, *105*, 1547–1562.
- (24) Pellegrino, T.; Kudera, S.; Liedl, T.; Muñoz-Javier, A.; Manna, L.; Parak, W. J. *Small* **2005**, *1*, 48–63.
- (25) Xiong, Y.; Washio, I.; Chen, J.; Cai, H.; Li, Z.-H.; Xia, Y. *Langmuir* **2006**, *22*, 8563–8570.
- (26) Lim, B.; Carmago, P. H. C.; Xia, Y. *Langmuir* **2008**, *24*, 10437–10442.
- (27) Hoppe, C. E.; Lazzari, M.; Pardiñas-Blanco, I.; López-Quintela, M. A. *Langmuir* **2006**, *22*, 7027–7034.
- (28) Pardiñas-Blanco, I.; Hoppe, C. E.; Piñeiro-Redondo, Y.; López-Quintela, M. A. *Langmuir* **2008**, *24*, 983–990.
- (29) Sakai, T.; Alexandridis, P. *Langmuir* **2004**, *20*, 8426–8430.
- (30) Sakai, T.; Alexandridis, P. *J. Phys. Chem. B* **2005**, *109*, 7766–7777.
- (31) Chen, S.; Guo, C.; Hu, G.-H.; Wang, J.; Ma, J.-H.; Liang, X.-F.; Zheng, L.; Liu, H.-Z. *Langmuir* **2006**, *22*, 9704–9711.
- (32) Goy-López, S.; Castro, E.; Taboada, P.; Mosquera, V. *Langmuir* **2008**, *24*, 13186–13196.
- (33) Dong, J.; Chowdhry, B. Z.; Leharne, S. A. *Colloids Surf. A: Physicochem. Eng. Aspects* **2004**, *246*, 91–98.
- (34) Álvarez-Lorenzo, C.; González-López, J.; Fernández-Tarrío, M.; Sánchez-Macho, I.; Concheiro, A. *Eur. J. Pharm. Biopharm.* **2007**, *66*, 244–252.
- (35) González-López, J.; Álvarez-Lorenzo, C.; Taboada, P.; Sosnik, A.; Sánchez-Macho, I.; Concheiro, A. *Langmuir* **2008**, *24*, 10688–10697.
- (36) Longenberger, L.; Mills, G. *J. Phys. Chem.* **1995**, *99*, 475–478.
- (37) Millstone, J. E.; Métraux, G. S.; Mirkin, C. A. *Adv. Funct. Mater.* **2006**, *16*, 1209–1204.
- (38) Kan, C.; Zhu, X.; Wang, G. *J. Phys. Chem. B* **2006**, *110*, 4651–4656.
- (39) Ah, C. S.; Yun, Y. J.; Park, H. J.; Kim, W.-J.; Ha, D. H.; Yun, W. S. *Chem. Mater.* **2005**, *17*, 5558–5561.
- (40) Li, C.; Cai, W.; Cao, B.; Sun, F.; Li, Y.; Kan, C.; Zhang, L. *Adv. Funct. Mater.* **2006**, *16*, 83–90.
- (41) Jin, R. C.; Cao, Y. C.; Hao, E.; Métraux, G. S.; Schatz, G. C.; Mirkin, C. A. *Nature* **2003**, *425*, 487–490.
- (42) Jana, N. R.; Gearheart, L.; Murphy, C. J. *Chem. Mater.* **2001**, *13*, 2313–2322.
- (43) Iwamoto, M.; Kuroba, K.; Zaporochentko, V.; Hayashi, S.; Faupel, F. *Eur. Phys. J. D* **2003**, *24*, 365–367.
- (44) Subramanian, C.; Tom, R. T.; Pradeep, T. *J. Nanoparticle Res.* **2005**, *7*, 209–217.
- (45) Sun, X.; Jiang, X.; Dong, S.; Wang, E. *Macromol. Rapid Commun.* **2003**, *24*, 1024–1028.
- (46) Liu, K.-J. *Macromolecules* **1968**, *1*, 308–311.
- (47) Yanagida, S.; Takahashi, K.; Okahara, M. *Bull. Chem. Soc. Jpn.* **1977**, *50*, 1386–1390.
- (48) Xie, J.; Lee, J. Y.; Wang, D. I. C.; Ting, Y. P. *Small* **2007**, *3*, 672–682.
- (49) Sakai, T.; Alexandridis, P. *Nanotechnology* **2005**, *16*, S344–S353.
- (50) Newman, J. D. S.; Blanchard, G. J. *Langmuir* **2006**, *22*, 5882–5887.
- (51) Paik, W. K.; Genshaw, M. A.; Bockris, J. O'M. *J. Phys. Chem.* **1970**, *74*, 4266–4275.
- (52) Sakai, T.; Enomoto, H.; Torigoe, K.; Sakai, H.; Abe, M. *Colloids Surf. A: Physicochem. Eng. Aspects* **2009**, *347*, 18–26.
- (53) Ha, T. H.; Koo, H. J.; Chung, B. H. *J. Phys. Chem. C* **2007**, *111*, 1123–1130.
- (54) Warshawsky, A.; Kalir, R.; Deshe, A.; Berkovitz, H.; Patchornik, A. *J. Am. Chem. Soc.* **1979**, *101*, 4249–4258.

JP908569Z